Microstructured Multilayered Surface-Acoustic-Wave Device for Multifunctional Sensing

H. Mishra, M. Hehn, Sami Hage-Ali, S. Petit-Watelot, P. Mengue, S. Zhgoon, H. M'jahed, D Lacour, O. Elmazria

Micro-structured, multi-layered surface acoustic wave device for multifunctional sensing

H. Mishra[1*], M. Hehn[1], S. Hage-Ali[1], S. Petit-Watelot[1], P. W. Mengue[1], S. Zghoon[2], H. M'Jahed[1], D. Lacour[1] and O. Elmazria[1#]

[1]*Institut Jean Lamour, Université de Lorraine, UMR CNRS 7198, F-54000, Nancy, France*
[2]*National Research University, Moscow Power Engineering Institute, 14 Krasnokazarmennaja, 111250 Moscow, Russia*
*harshad.vr1@gmail.com; #omar.elmazria@univ-lorraine.fr

A multifunctional sensor based on a surface acoustic wave (SAW) device has been fabricated. It allows independent measurements of temperature and applied magnetic field. Optimization of the multilayered device structure leads to a temperature coefficient frequency of the Love wave resonance reduced to zero. The sensitivity to an applied magnetic field is obtained through magnetostriction of a CoFeB layer. By use of shape anisotropy, the variation of intrinsic magnetic anisotropy with temperature is strongly reduced. On one hand, interrogating the device at the Love wave resonance frequency allows to extract the applied magnetic field independently of the temperature in a [130 - 370K] range. On the other hand, the Rayleigh or Leaky waves are less or not sensitive to applied fields but have a high temperature coefficient of frequency. So interrogating the device at the Rayleigh resonance frequency allows to extract the temperature independently of the magnetic field. In addition, the used resonator geometry offers the possibility for future battery less and wireless interrogation.

I. Introduction

Due to their sensitivity to different chemical and physical stimuli, Surface Acoustic Wave (SAW) devices offer excellent capabilities as sensors [Aub10, Tal06, Woj79]. The addition of a magnetostrictive material into the SAW structure allows the magnetic SAW (MSAW) to probe the magnetic field through the magnetostrictive strains and changes to the elastic constants [Kad11, Elh16, Tie08, Pol17, Mis19, Web79, Zho14]. Several studies have been devoted to the magnetic field sensitivy optimization through the device geometry or the choice of material [Zho14, Kitt18]. Progresses towards the use of different elastic waves to improve the magnetic field sensitivity have also been made [Kitt18, Maz20]. However, these studies do not take into account thermal effects. A sensitivity to multiple stimuli, each coupled with the others constitutes a source of complexity when interpreting the output signal of a sensor. A major challenge in magnetic field measurements lies in the large temperature coefficient of frequency (TCF) of SAW devices. From the perspective of applications of MSAW devices, this becomes extremely detrimental, not only in the case of

strong temprature variations, but also in an environment where the temperature fluctuates. In addition to the TCF, the magnetic anisotropy controlling the magnetization response under applied field can also be strongly temperature dependent. Generally, an increase in temperature leads to a increase in the internal energy of the ferromagnetic material by virtue of a rise in its entropy and therefore leads to a decrease of the anisotropy constants [Get07]. Magnetocrystalline anisotropy, strain induced anisotropy and magnetic field induced anisotropy are all strongly dependent on temperature, either in their intensity or in their direction. As a result, the MSAW response can be strongly altered by the temperature in many ways. Thus, it becomes a prime concern to nullify the effects of temperature on both the magnetic properties and the TCF if we intend to develop an MSAW sensor that is genuinely compensated for temperature in a practically wide temperature range.

There have been several studies aimed at improving the limit of detection (LOD) of SAW devices for magnetic field sensing that are based on extensive phase noise analysis and aim to improve the signal to noise ratio [Kitt18, Dur18]. These studies are primarily focused on the development of sensor systems including electronic ciruits that optimize the performance of SAW based magnetic field sensors. On the other hand, improving the quality factor (Q) of the SAW device by optimizing its design also leads to enhancement of the LOD. Our focus in this work has been the development of a truly multifunctional SAW sensor that can in future be integrated with such electronic sensor systems to operate wirelessly, and hence we do not discuss the LOD of our devices but rather focus on the structure of the device and the physics behind it.

In our study, we propose a multilayered device structure capable of eliminating the effects of temperature on both the resonance frequency and on the magnetic anisotropy of the sensitive layer. First of all, the positive TCF of a ST-cut quartz crystal has been compensated for by the negative TCF of a ZnO insulating layer. The optimization of its thickness led to a near- zero TCF for the guided Shear wave, i.e. the Love wave. Secondly, we decided to use shape induced anisotropy to influence the anisotropy of a CoFeB magnetostrictive layer. The magnetization of ferromagnetic materials varies only by several % when the temperature is far from its Curie temperature, and thus the anisotropy direction remains unchanged and the intensity of the anisotropy constant varies only by a few % in the [130 - 370K] temperature range. In a previous study, we had shown that the intensity of the anisotropy constant can easily be changed by altering the aspect ratio of the CoFeB nanostructures [Pol17]. As a result, the resonator-based device is shown to have three resonances: a Rayleigh wave which is sensitive to temperature and partially sensitive to a magnetic field, a Love wave which is not sensitive to temperature but highly sensitive to magnetic field and a Leaky wave that is highly sensitive to temperature but not to a magnetic field. Based on this, we propose a multifunctional device, enabling the detection of magnetic field as well as temperature simulataneously, yet being independent of each other.

II. Device fabrication

The substrate are single sided polished 42.75° Y rotated ST-cut quartz crystals. The SAW devices have a resonator geometry with a wavelength (λ) of 10µm and a metallization ratio of 50%. The wave propagation direction is chosen along the (X+90°) direction. We fabricated the electrodes and the connecting pads from a 100nm thick Aluminium layer using conventional optical lithography and a lift-off based process. Subsequently, a ZnO thin insulating layer has been deposited onto the device, as a rectangular area covering the device using a lift-off technique. Based on previous optimization studies [Mis20], three ZnO thicknesses of 200nm, 400nm and 600nm were deposited on the devices. The deposition of the ZnO layer was carried out by RF sputtering of a 4-inch ZnO (oxygen rich) target at 150W with 3×10^{-3} mbar and 8 cm^3/min flow rate of both Ar and O_2. Finally, using UV lithography, the photoresit layout for deposition of the CoFeB strip structure on top of the ZnO layers was designed as multiple rows of 1.5µm × 500µm bars covering an area of 3120µm × 710µm with a gap of 1µm between each strip. The 100nm blanket or thin film of CoFeB was then deposited by RF sputtering of a 3-inch target at 300 W and 5×10^{-3} mbar Ar and the lift-off was performed. Figure 1 (a) shows a schematic of the fabricated device. We also fabricated a multilayered structure of 4mm×4mm dimension, that corresponds exactly to the multilayered structure of the SAW device, but without the Al electrodes, a schematic of which is presented in Figure 1 (b). This sample was fabricated to conduct rigorous magnetometry tests.

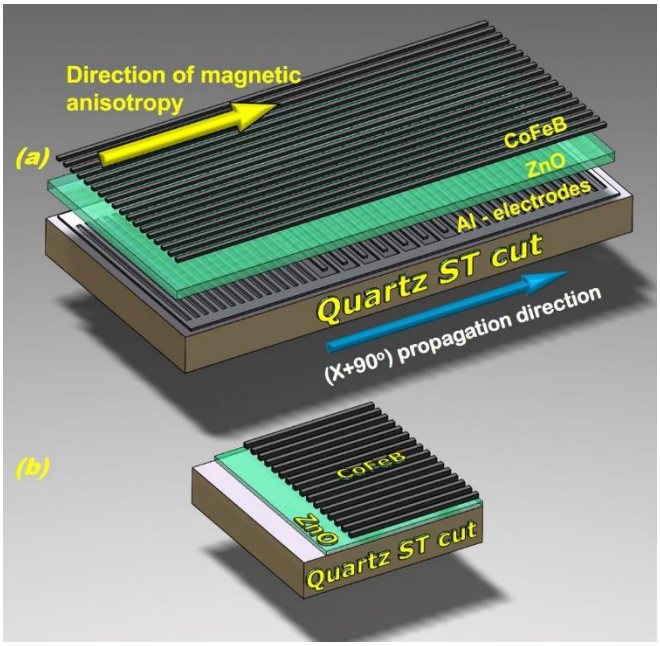

Figure 1: (a) Schematic of the fabricated MSAW device and (b) the magnetometry sample.

The topography of the fabricated MSAW device was studied using MFP-3D Infinity Atomic Force Microscope (AFM). Figure 2 summarizes the analysis of the surface of the device with 400nm thick ZnO. As shown in figure 2a, the purple segment shows the location of one IDT of the SAW structure and the green segment shows the location of one CoFeB strip. Of course, the IDT electrodes and the CoFeB strips are separated by 400nm of the ZnO layer to avoid electrical short cuts. The first thing that becomes very apparent with the above figure is the rabbit's ear structure. This is a very peculiar structure that often occurs due to the lift-off procedure leading to the deposition of material on the resist side walls. As can also be seen, the rabbit's ear of the Al electrodes are higher in the region covered by the CoFeB strip meaning that the CoFeB strip is continuous over the Al electrodes. Figure 2(b) gives an analysis of the surface heights along two cross sections. The red area shows the strong imprint of the Al electrodes even at the top surface of the ZnO layer. As mentioned earlier the electrodes are fabricated from 100nm of Al. However, despite depositing 400nm of ZnO over the electrodes, an imprint of 77nm was very clearly measured. This gives a qualitative idea about how undulating the surface of the ZnO is. The blue area gives the thickness of the CoFeB, deposited to form the micro-structured magneto-sensitive layer which is measured to be 97nm as expected. Finally, the width of the Al electrodes was estimated to 2.53µm while the width of the CoFeB strip was measured to be 1.36µm.

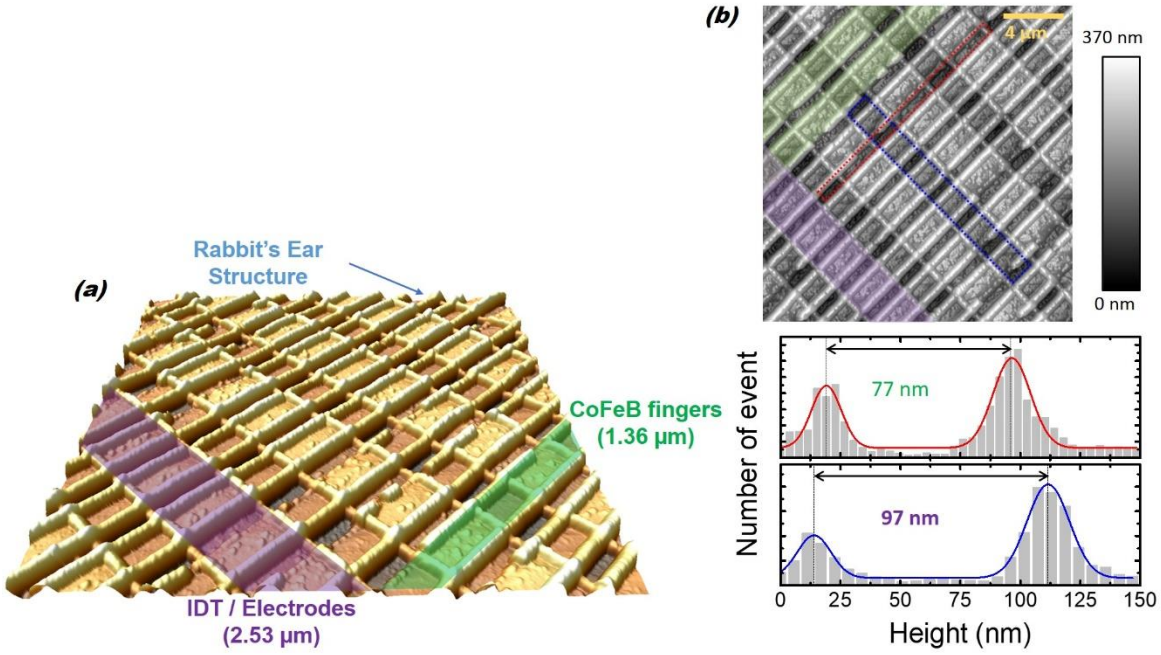

Figure 2: (a) Surface topography over a section of device with 400nm of ZnO.(b) Cross sections done on the surface of the device with 400nm of ZnO, using the atomic force microscope. The 'impression' of the Aluminium IDTs (100nm thick) on the 400nm ZnO layer is measured at 77nm while the thickness of the CoFeB layer is measured at 97nm.

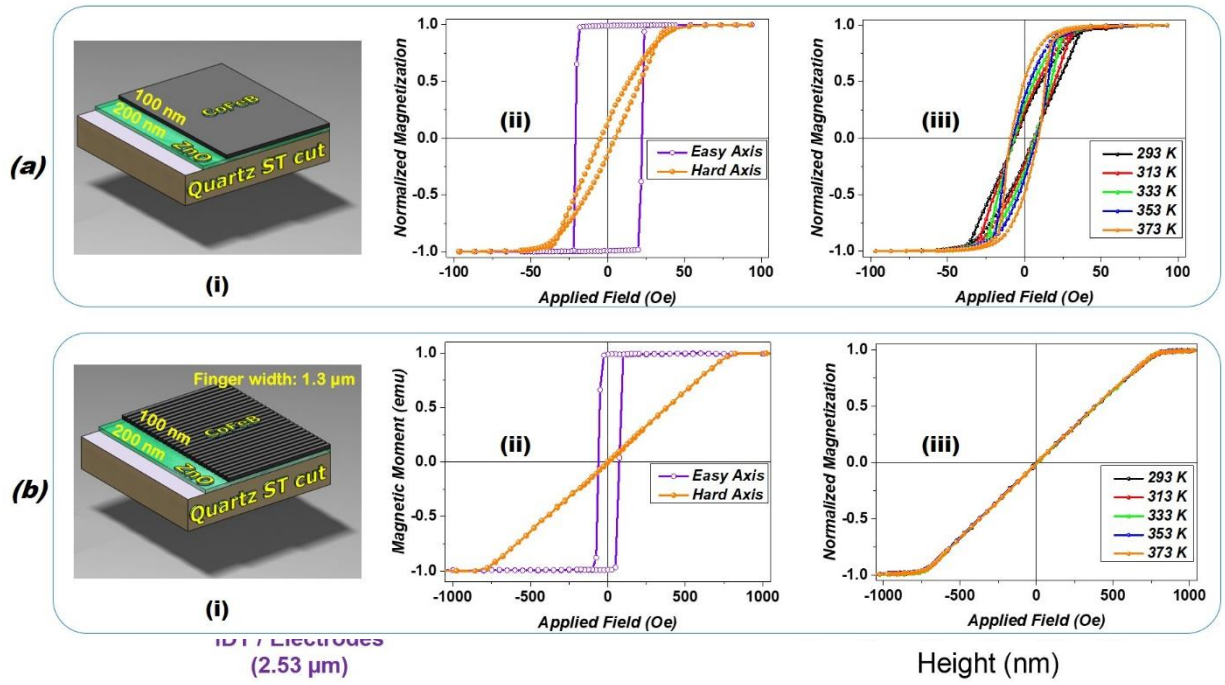

Figure 3: Normalized magnetization measurements conducted on different samples (a) Full film of CoFeB deposited on 200nm of ZnO; (b) CoFeB strips of 1.36µm width on 200nm of ZnO.

III. Magnetometry measurements

One of the key aspects to control the magnetic response of the sensor consists in studying the response of the magnetization under an applied magnetic field. Therefore, the magnetic properties of a 100nm thick CoFeB film deposited on top of 200nm of ZnO have been measured. Figure 3 (a-ii) shows undoubtedly the presence of an easy axis of magnetization (square hysteresis curve) and a hard axis that is perpendicular to the easy axis direction. The origin of this magnetic anisotropy relies either on the strain imposed by the ZnO layer on the CoFeB during growth or on the magnetron stray field during the CoFeB growth. The response along the hard axis is hysteretic around zero applied field. This hysteresis is a priori redhibitory for the realization of a magnetic field sensor. Furthermore, we measured the hard axis response for temperatures ranging from 293 K to 373 K as reported in figure 3 (a-iii). As can be seen, the saturation field decreases by a factor of two when temperature increases from 293 to 373 K. This is a clear evidence that the anisotropy of the full film decreases by a factor of two. Indeed, in the same temperature window, the saturation magnetization, Ms, only varies by 2.1%. This change of saturation field with temperature and the presence of the hysteresis renders this CoFeB layer ineffective for our MSAW sensor.

Considering the small variation of Ms with temperature, we decided to define micro-structures in the magnetostrictive layer with an aspect ratio such that the magnetic anisotropy of CoFeB is provided by the shape anisotropy that varies as Ms. A variation of anisotropy with temperature

less than 2.1% is then expected. Furthermore, reducing the width of the CoFeB strip will ensure a more homogenous magnetization rotation and should decrease the magnetic hysteresis.

The width of the strips was measured at 1.36 µm after fabrication. Figure 3 (b-ii) depicts the measurements along the easy and hard magnetization direction. As expected, a clear observation of the easy axis is made along the length of the strips. The hard magnetization axis lies perpendicular to the length of the strips. A trade-off for the control of the magnetization is the increased saturation field, its value can be adjusted by the strip aspect ratio. Measurements of the magnetization (refer Figure 3 (b-iii)) at different temperatures show that micro-structuration enables us to obtain a magnetic response that does not change in the 293 K – 373 K temperature window. Consequently, by introducing shape anisotropy to control the magnetization in the magnetostrictive layer, we have successfully addressed and found a way to supress the temperature sensitivity of the magnetic anisotropy. Furthermore, the magnetic response is not only stable up to 373 K, but also presents a macro-spin response akin to the ideal magnetization proposed by the Stoner-Wohlfarth model. Combined with the multi-layered device geometry, this crucial factor will now enable us to develop devices which are truly compensated for the effects of temperature. On the other hand however, with respect to the full film situation, the strain induced by the magnetization rotation will certainly lead to a reduction of the MSAW frequency variation with applied field, thereby leading to a comparatively less sensitive device.

IV. RF characterization and TCF measurement

Figure 4a presents the S_{11} return loss spectrums for the devices with 200nm, 400nm and 600nm of ZnO along with 100nm of micro-structured CoFeB layer over it. As can be noted, the S_{11} signal from device with 200nm of ZnO is very small compared to the signals from the two other devices. The reason for this was investigated. The low ZnO thickness is causing electrical losses in the device to due proximity effect between the metallic CoFeB and the electrodes. Four resonance frequencies are observed on the devices. In order to validate the nature of the resonance frequencies, we conducted a simulation-based analysis of the deformations associated with each resonance.

The simulations shown in figure 5 have been obtained on the device with 400nm of ZnO. As can be clearly seen, the first resonance peak (329 MHz) corresponds to a Rayleigh wave while the second resonance peak (421 MHz) corresponds to a Love wave. On the other hand, a tiny peak is observed at 431 MHz, that appears to be a mixed mode resonance. Finally, a fourth resonance is observed at 566 MHz. It is interpreted as a Leaky wave. Since the Love wave absorption peak has been identified, we measured the TCF of the Love wave in the various devices and they are reported in figure 4 (b). A clear variation of the TCF can be observed with changing thicknesses of the ZnO layer; wherein, 400nm emerges as the best choice to annihilate the impact of temperature on the amplitude of the frequency response of the Love wave to the strain induced by the CoFeB (TCF of -1.65 ppm/K). On the other hand, this choice of ZnO thickness does not

annihilate the response of the Rayleigh and Leaky waves to temperature. Having thus determined the particular device that is best suited for our study (involving Love waves), we also measure the individual TCFs of each remaining resonance peak in this device comparing them the TCF of the Love wave resonance. As shown in figure 6, the first peak that corresponds to a Rayleigh wave has a TCF of -46 ppm/K and while the last peak that corresponds to a Leaky wave has a TCF of -99 ppm/K. If their response does not depend on the magnetic state of the CoFeB, they could give a measure of the temperature of the device. Comparatively the Love wave resonance in the same device should allow the measurement of magnetic field without any temperature effects.

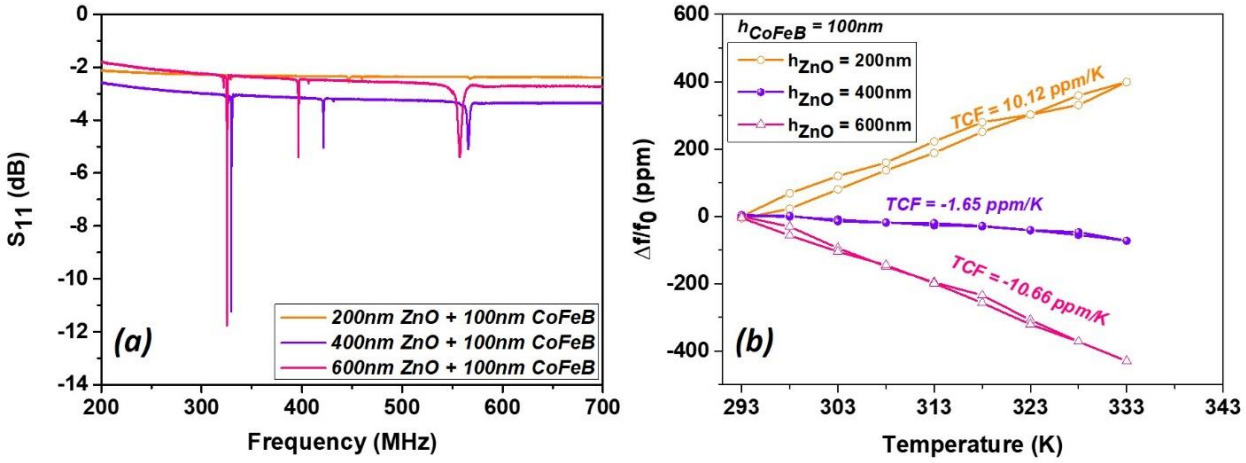

Figure 4: (a) Scattering parameter (S11) measured on samples with different ZnO thicknesses after deposition and micro-structuration of 100nm of CoFeB; (b) TCF measured on the Love wave resonances in the three devices.

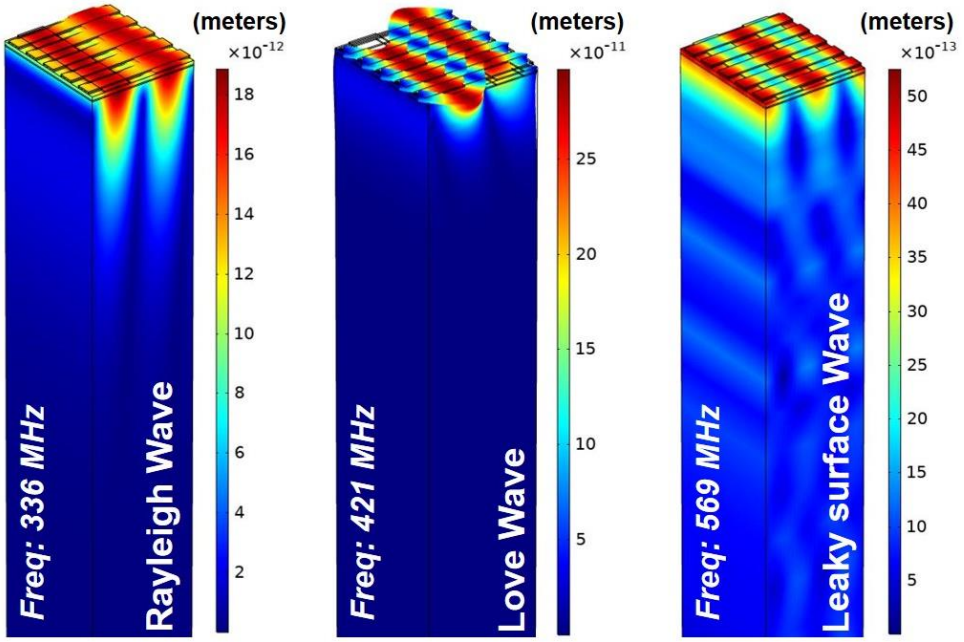

Figure 5: Total displacements observed for the different resonance frequencies in device with 400nm ZnO as obtained through COMSOL simulations.

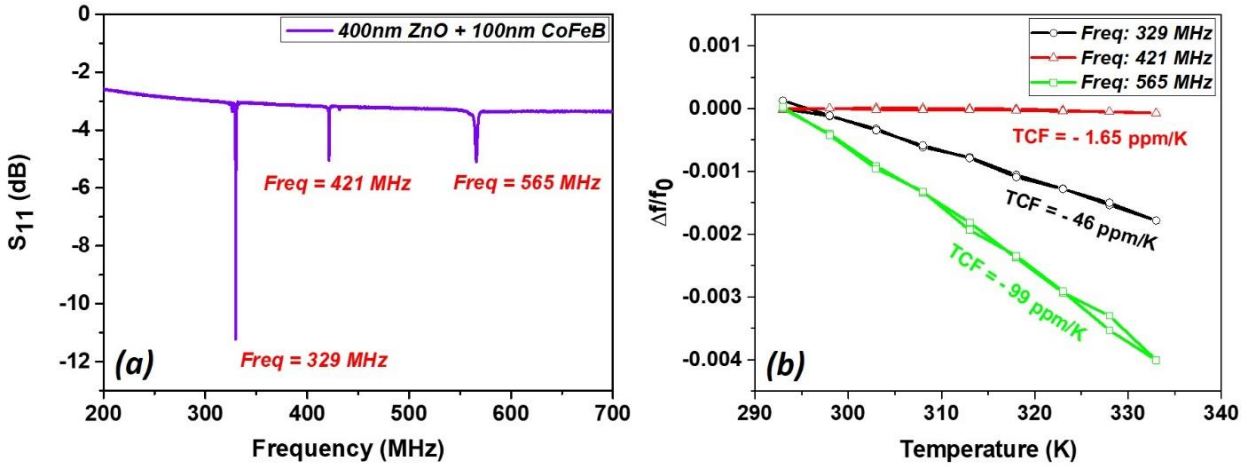

Figure 6: Scattering parameter (S_{11}) measured on samples with 400nm of ZnO after the deposition and micro-structuration of 100nm of CoFeB. For each wave, the values of the TCF have been added.

V. Magneto-acoustic measurement

In this section, we study the variations of the Love wave resonance frequency with respect to the intensity of an external magnetic field applied along the hard magnetic axis (figure 7a). In the previous section, we optimized the thickness of the layers to get a zero-TCF structure using 400nm of ZnO and 100nm of CoFeB. Therefore, in this section we consider only this device and study the magneto-acoustic response for the Rayleigh, the Love and the Leaky wave resonance frequencies observed. The MSAW measurements were made using a LakeShore cryogenic probe station (EMPX-HF) connected to a Vector Network Analyzer (VNA: Rohde and Schwartz ZVA67) by a K-cable and a GGB Picoprobes (40 GHz) probe head. During the measurement, the device is placed between the electromagnets in a vacuum sealed chamber, to ensure a thermally stable and isolated environment. The water-cooled electromagnets are capable of providing a bi-directional magnetic field up to 6000 Oe.

The first measurement of the magneto-acoustic response is made on the temperature compensated Love wave observed at 421 MHz (figure 7b). A first important aspect to note here is also the relative absence of a hysteretic behavior. This is achieved because of the exceptional control over the magnetic properties of the CoFeB layer through micro-structuration. Subsequently, in order to validate the magneto-acoustic sensitivity of the Love wave resonance in the device as independent of temperature, we conducted measurements over a wide range of temperatures. The experimental setup for this was the same as described previously; although, we modified the system to a liquid Nitrogen based cooling system for control of the temperature. Figure 7b presents the measurements of the magneto-acoustic response of the device when the field is increased from -5000 Oe to +5000 Oe. As can be clearly seen, the responses appear quite stable and despite a temperature variation of almost 200 K, the resonance frequency without any magnetic field almost does not shift from

421 MHz. It needs to be noted here that although we had measured the TCF of this frequency at around -1.65 ppm/K, it was between 293 K and 333 K. There remains a possibility that this value may differ marginally at cryogenic and high temperatures. Additionally, considering that the temperature was maintained manually by optimizing the flow of liquid N_2, a variation of around 4 K was observed even during the measurements. Further, the calibration of the setup was only done at room temperature, whereas in order to optimize the responses, it was essential to have a calibration at each temperature. The effects of all of these shortcomings can be seen as noise and minor differences seen in figure 7b. However, despite all the challenges, we can see that in the linear region that is of importance for device applications (approximately between 500 Oe and 1000 Oe), the MSAW responses of all the devices corroborate with negligible differences. This renders the device a highly stable performance from cryogenic to high temperatures thereby greatly expanding the possible areas of applications.

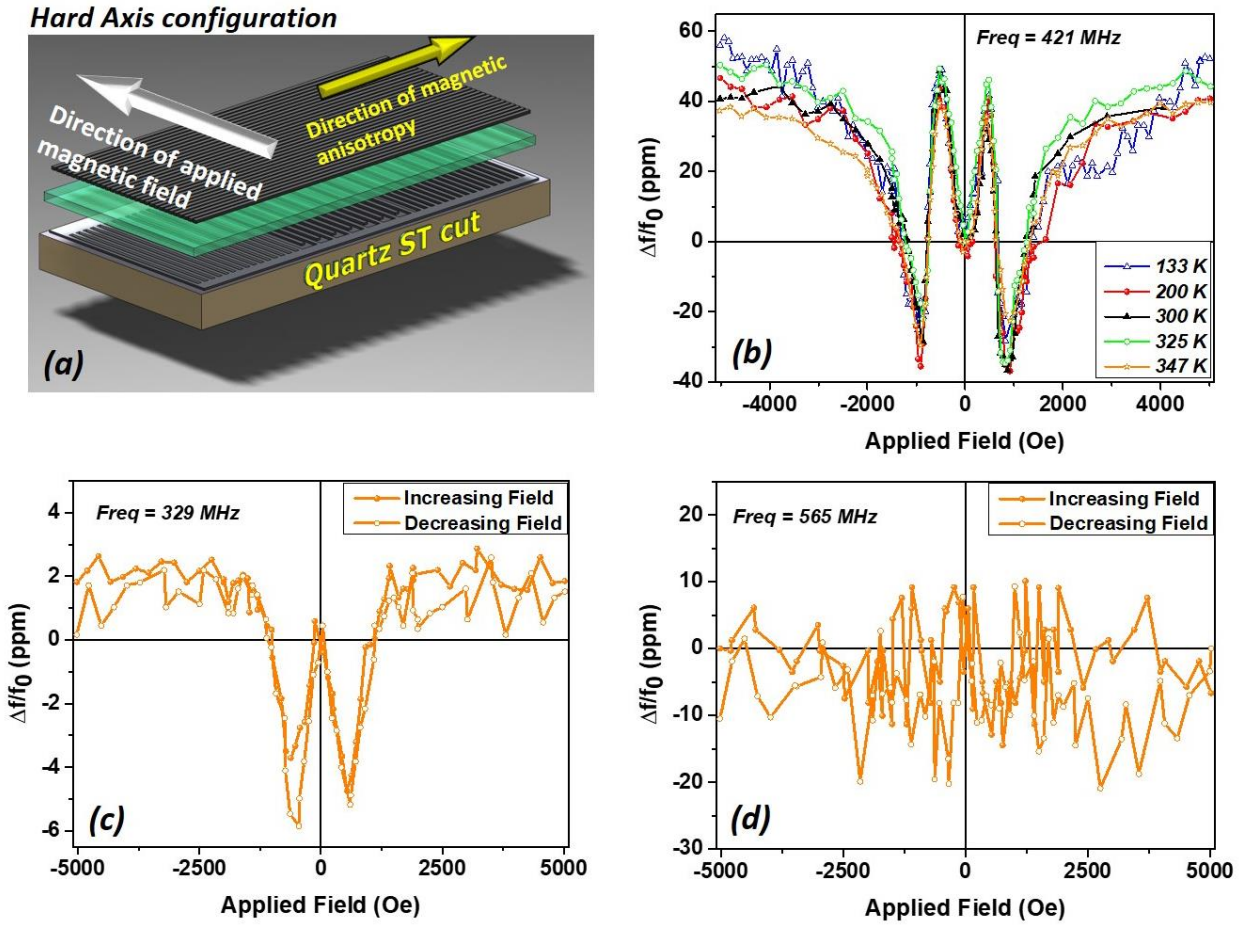

Figure 7: Magneto-acoustic response of the Love wave peak in device with 400nm of ZnO for a magnetic field applied along the hard axis (perpendicular to the CoFeB strips) (a) the geometry of measure; (b) Magneto-acoustic response of the Love wave at different temperatures; (c) Magneto-acoustic response of the Rayleigh wave; (d) Magneto-acoustic response of the Leaky

In order to complete the magneto-acoustic characterization of the device, we also measured the magneto-acoustic response of the Rayleigh wave and Leaky wave peaks. Figure 7c presents the response of the Rayleigh wave peak. The characteristic 'W-shaped' curve provides a much smaller response as compared to the Love wave in the same device. This low sensitivity to magnetic field, combined with a high sensitivity towards temperature (-46ppm/K) enables the device to be considered as a multifunctional platform to sense magnetic field as well as temperature, both relatively independent of each other. The same conclusion can be held for the Leaky wave (figure 7d). Since we already understand that these secondary resonances are not temperature compensated (non-zero TCF), their responses to magnetic field at different temperatures were not measured.

VI. Conclusions

In this research work, we addressed a major concern to mitigate the effects of temperature on a SAW device used for magnetic field sensing. First of all, the positive TCF of the quartz-based device is compensated by utilizing a multi-layered structure of ZnO and CoFeB. Further, the CoFeB layer was micro-structured in the form of strips to overcome the effects of temperature on the magnetic anisotropy. Additionally, through magnetometry analysis, we have revealed that the device exhibits a hysteresis free behavior. Among the different relevant resonances that were observed in the device at different frequencies, one is related to a Rayleigh or a Leaky wave, sensitive to temperature and negligibly sensitive to a magnetic field; while the second, is a Love wave, with a negligible sensitivity to temperature (-1.65 ppm/K) and a high sensitivity to magnetic field (0.75 MHz/T). Finally, measurements of the magneto-acoustic response at different temperatures validate the capability of our device to operate in temperatures ranging from cryogenic to relatively high temperatures. Thus, in this work, we have demonstrated the capability to develop the SAW device as a multifunctional sensor capable of detecting magnetic field as well as temperature at the same position and each, independent of the effect of the other. As a result, we have established a new state-of-the-art technology for SAW devices to be multifunctional encompassing magnetic field sensitivity and temperature sensitivity in the same device.

Acknowledgements

We would like to acknowledge the support from the French PIA project "Lorraine Université d'Excellence" (ANR-15-IDEX-04-LUE) and by the Région Lorraine, ANR JCJC SAWGOOD (ANR-18-CE42-0004-01) the European funds FEDER. Experiments were carried out on IJL Project TUBE-Davm equipment funded by FEDER (EU), Region Grand Est, Metropole Grand Nancy. We also extend our sincere gratitude to the staff from the Competence Centre MINALOR for helpful discussions in fabrication.

References

[Aub10] Aubert T., Elmazria O., Assouar B., Bouvot L., and Oudich M., 2010, Appl. Phys. Lett. 96, 203503

[Tal06] Talbi A., Sarry F., Elhakiki M., Le Brizoual L., Elmazria O., Nicolay P., and Alnot P., 2006, Sens. Actuators A Phys, 128, 78

[Woh79] Wohltjen H. and Dessy R., 1979, Anal. Chem. 51 (9) 1458–1475

[Kad11] Kadota M., Ito S., Ito Y., Hada T., and Okaguchi K., 2011, Jpn. J. Appl. Phys. 50, 07HD07

[Elh16] M. Elhosni, O. Elmazria, S. Petit-Watelot, L. Bouvot, S. Zhgoon, A. Talbi, M. Hehn, K. Ait-Aissa, S. Hage-Ali, D. Lacour, F. Sarry, O. Boumatar ; 2016, Sens. Actuator A Phys, 240, 41–49

[Tie08] Tiercelin N., Talbi A., Preobrazhensky V., Pernod P., Mortet V., Haenen K., and Soltani A., 2008 Appl. Phys. Lett. 93, 162902

[Pol17] Polewczyk V., Dumesnil K., Lacour D., Moutaouekkil M., Mjahed H., Tiercelin N., Petit Watelot S., Mishra H., Dusch Y., Hage-Ali S., Elmazria O., Montaigne F., Talbi A., Bou Matar O., Hehn M., 2017, Phys. Rev. Appl. 8, 024001

[Mis19] Mishra H., Hehn M., Lacour D., Elmazria O., Tiercelin N., Mjahed H., Dumesnil K., Petit Watelot S., Polewczyk V., Talbi A., Bou Matar O., Hage-Ali S., 2019, Smart Mater. Struct. 28, 12LT01

[Web79] Webb D. C., Forester D.W., Gangu1y A. K., and Vittoria C., 1979 IEEE Trans. Magn. 15, 1410

[Zho14] Zhou H., Talbi A., Tiercelin N., and Bou Matar O., 2014 Appl. Phys. Lett. 104, 114101

[Kitt18] Kittmann A., Durdaut P., Zabel S., Reermann J., Schmalz J., Spetzler B., Meyners D., Sun N. X., McCord J., Gerken M., Schmidt G., Höft M., Knöchel R., Faupel F. and Quandt E., 2018 Scientific Reports, 8, 278

[Get07] Mathias Getzlaff, “Fundamentals of Magnetism”, ISBN 978-3-540-31150-8 Springer Berlin Heidelberg New York.

[Dur18] Durdaut P., Hoft M., Friedt J-M., Rubiola E., 2019, Sensors 19(1), 185.

[Mis20] Mishra H., Streque J., Hehn M., Mengue P. W., Mjahed H., Lacour D., Dumesnil K., Petit-Watelot S., Zhgoon S., Polewczyk V., Mazzamurro A., Talbi A., Hage-Ali S., Elmazria O., 2020, Smart Mater. Struct. 29

[Maz20] Mazzamurro A., Dusch Y., Pernod P., Bou matar O., Addad A., Talbi A., Tiercelin N., 2020, Phys. Rev. Appl. 13 044001